Evaluation of Drop Size Distribution from Chord Length Measurements

Bin Hu
Dept. of Chemical Engineering, University College London, London, U.K.; and Dept. of Chemical Engineering, Imperial College London, London, U.K.

Panagiota Angeli
Dept. of Chemical Engineering, University College London, London, U.K.

Omar K. Matar, Christopher J. Lawrence, and Geoffrey F. Hewitt
Dept. of Chemical Engineering, Imperial College London, London, U.K.

DOI 10.1002/aic.10714
Published online November 4, 2005 in Wiley InterScience (www.interscience.wiley.com).

The relationship between the chord length distribution (CLD) obtained by a point sensor and the drop size distribution (DSD) in a liquid-liquid dispersion is investigated. Based on analysis of the frequency of drop-cuttings by the sensor, a physical model is built to derive the probability density function of chord lengths for a given DSD, and vice versa. The effect of biased sampling towards larger drops relevant to point sensors, which is often ignored by investigators, is included in this relationship. A new algorithm is introduced to solve the problem of noisy or even negative DSD values by adding smoothing equations while performing the backward conversion. The effects of parameters, such as the number of drop size groups used, the noise level, and the smoothing factor value, on the backward transform are further studied. Both forward and backward transforms are shown to be in good agreement with ideal data when using continuous (e.g., log-normal, uniform) distributions and with data obtained from Monte-Carlo simulations. Good agreement is also found between the DSD obtained from chord length measurements and drop size data determined by direct observation. *AIChE J,* 52: 931–939, 2006
Keywords: drop size distribution, chord length distribution, two-phase, dispersed flow, measurement

Introduction

Dispersed (or bubbly) flows where one fluid (such as oil or air) is dispersed in the other continuous fluid (such as water) in the form of drops or bubbles occur very often in multiphase flow systems in the chemical, pharmaceutical and oil industries. One important characteristic of dispersed flow behavior is the distribution of drop (or bubble) sizes, which has been found to affect significantly the heat/mass transfer and turbulence characteristics. Many experimental techniques for drop size measurement have been developed for air-liquid and liquid-liquid systems: photographic and video recording techniques,[1] sometimes coupled with an endoscope to obtain local measurements[2]; resistance or impedance probes[3,4]; hot-film anemometry[5]; and optical probes, such as the Par-Tec 300, Lasentec Ltd.[6,7] However, while photographic and video recording techniques give the drop diameter distribution directly, other techniques involving point sensor probes provide only a distribution of the chord lengths intersected by the probe. It is, therefore, necessary to convert a measured chord length distribution (CLD) to the relevant drop size (diameter) distribution (DSD).

Correspondence concerning this article should be addressed to P. Angeli at p.angeli@ucl.ac.uk.

Consider a dispersed system where the drops (or bubbles) are uniformly distributed in space and the distribution of drop size R is described by $P(R)$. The chord length distribution $P(L)$, defined as the likelihood of finding chords of length L among all the intersected chords, will be determined by the following factors:

(A) the size distribution function $P(R)$ of drops in the system;

(B) the conditional probability function $P(L|R)$ of cutting a chord of length L from a drop intersected by the probe with a specific size R;

(C) the biased sampling probability function $P_B(R)$, which describes the likelihood that a drop of size R will be sampled by the probe if a uniform spatial distribution is assumed. This is known as biased sampling because the probe is more likely to sample large drops than small ones, as will be shown below.

Knowing the above functions, the distribution function of the measured chords $P(L)$ for any system can generally be written as follows:

$$P(L) = \int_0^\infty P(L|R)\,P_B(R)\,P(R)\,dR = \int_{L/2}^\infty P(L|R)\,P_B(R)\,P(R)\,dR \quad (1)$$

where the latter equality follows since $P(L|R)$ is zero for $R < L/2$. Note that the probability functions $P(L|R)$, $P_B(R)$, and $P(R)$ are independent of each other, while the values of $P(L|R)$ and $P_B(R)$ depend on the sensor geometry (e.g., needle-tip probe, optical sensor, or laser sheet), the drop shape, and the drop motion (e.g., uni- or multi-directional flow), and can be calculated accordingly, while $P(R)$ is a property of the dispersion. The function $P(L|R)$ has been calculated by Clarke and Turton[8] for various bubble shapes in a uni-directional flow. In the present work, we consider only spherical drops and point probes, for which $P(L|R)$ is independent of the details of the flow. In this case, $P_B(R)$ is independent of the directionality of the flow; it could be influenced by a variation of the droplet speed with R, but we shall assume that all drops have the same speed. These assumptions are consistent with the analysis of drop size distribution in dispersed oil/water pipe flows.

Equation 1 describes the forward transformation from DSD to CLD. It can also be used to obtain the system DSD from an experimentally measured CLD (known as backward transformation). To the best of the authors' knowledge, Eq. 1 has not been used explicitly before, although the concept of biased sampling with respect to larger drops has been considered by other investigators and expressions similar to Eq. 1 have been reported in some studies that combined $P_B(R)$ and $P(R)$ into a sampling distribution function $P_P(R)$.[8-10] Langston et al.[11] also mentioned that the probability of a particle being detected depends on its size. Wynn[12] derived a relationship between DSD and CLD that included the effect of biased sampling based on geometrical arguments that related the drop position to that of the probe.

The backward transform from CLD to DSD is usually achieved by discretizing Eq. 1 in a matrix form and directly solving it (e.g., [8,12]). In addition, a number of methodologies have been suggested for finding the DSD from the CLD, such as the peeling method (PM)[13]; the probability apportioning method (PAM),[7] which was found to be in error and was later improved to PAM2[11]; and the finite element method (FEM)[7]. Recently, techniques that describe more complicated systems, such as ellipsoidal bubbles with multi-dimensional motion[14] and spherical bubbles with size-dependent velocity,[15] have also been proposed. However, neither of these works fully incorporated the effect of $P_B(R)$.

Apart from the form of the relation between CLD and DSD, previous studies have also been concerned with the stability of the backward transformation (from measured CLD to system DSD). Clarke and Turton[8] assessed the backward-calculated $P(R)$ using the CLD $P(L)$ generated by Monte-Carlo simulations from a given DSD and found that the results are sensitive to the number of groups (bins) that the drop diameter data are divided into. If the number of groups is increased beyond some value, the backward transform becomes unstable, yielding irregular and sometimes negative $P(R)$ values. For the "peeling" method suggested by Hobbel et al.,[13] Simmons et al.[7] found that the converted $P(R)$ is very sensitive to the "noise" in the population of the largest size. Their own PAM model was found to be always stable and agreed reasonably well with simulated drop size data but was inaccurate for unknown drop diameters. The improved PAM2 model[11] was found to be more accurate and robust when applied to the experimental data measured from a Lasentec ™ Par-Tec optical instrument. Simmons et al.[7] also noted that the FEM model is robust in general cases when the drop diameters are not known but inaccurate for discontinuous CLD data due to overshoot in the numerical integration and, consistent with the findings by Clark and Turton,[8] negative values were often observed.

Recently, Wynn[12] proposed a model to study the relationship between drop size and chord length measured by a Lasentec™ focused beam reflectance instrument. By integrating the probability that the beam cuts chords of one size from the passing drops of various sizes, a matrix equation was deduced. The drop size distribution was then calculated by solving this equation. However, as the method of solving the matrix equation is equivalent to the earlier "peeling" method, it is very sensitive to errors in the counting of large drops and negative results are unavoidable. After testing the matrix equation, it was suggested that the model may show reasonable stability if the drop size intervals are chosen to be very small. In addition, Liu et al.[10] developed a 2-D conversion relationship in a heterogeneously dispersed system based on the assumption that the DSD can be represented as the product of two functions that are only dependent on drop size and chord length. Interestingly, they also observed that the accuracy of the numerical backward transform was increased as the drop classification group number increased, which differs from the observation of Clark and Turton.[8]

In most of the previous work, biased sampling has not been properly considered while conceptual mistakes have sometimes been present. The backward transforms generally suffer from stability problems. In this article we reconsider the problem of inferring the DSD from the CLD and investigate the relationship through a direct method, as suggested by Wynn,[12] to include the effect of biased sampling. To this end, both forward and backward calculations are carried out, and a new algorithm

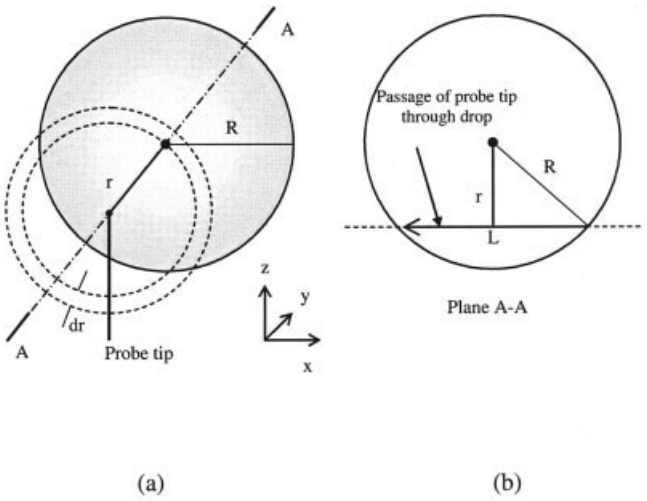

Figure 1. Drop sampled by "needle" probe.

(a) View of x-z plane at point of closest approach, (b) Intersecting path with chord length L in plane A-A.

is postulated for eliminating the previous problem of sensitivity to noise and negative DSD values. A dispersed system is considered with spherical drops (or bubbles) that move at a constant speed.

Mathematical Relationship Between DSD and CLD

Models and equations

In this section, the relationship between DSD and CLD is investigated and deduced for two-phase systems where the chord lengths are obtained by a "needle" (point sensor) probe, for example, an impedance or conductivity probe. Here, we assume that drops with spherical shapes are homogeneously distributed and that drops of all sizes move with the same velocity. The dimension of the probe sensor tip is negligible compared to the drop size, and drops are assumed not to deform while passing across the probe. Therefore, the maximum chord length ($L_{\max}$) will be equal to the maximum drop diameter ($D_{\max}$). Figure 1a illustrates a drop of radius R that intersects the probe at a closest-approach distance r to the probe tip. In the diagram, the needle probe is oriented in the z-direction and the drop moves into the paper in the y-direction; r is the distance of closest-approach between the particle center and the probe tip, measured in the x-z plane. The arising chord length can then be calculated from the Pythagorean Theorem, as shown in Figure 1b, which leads to:

$$L = \sqrt{D^2 - 4r^2} \tag{2}$$

where L is the chord length intersected by the probe and $D = 2R$ is the drop diameter.

Here we can define the drop size distribution (DSD) of the system as a relative number density per unit volume, $P(D)$, where for drops with sizes between D and $(D + dD)$ the number density is $N_T P(D)dD$, in which N_T is the total number of drops per unit volume. Similarly, $X(r,D)dDdr$ is defined as the sampling frequency of drops of size between D and $D + dD$ at a central distance between r and $r + dr$ (see Figure 1a), which is given by:

$$X(r, D)dDdr = 2\pi r dr \cdot N_T \cdot P(D)dD \cdot U \tag{3}$$

where U is the velocity at which drops pass the probe. From Eq. 2 we also have:

$$r = \frac{\sqrt{D^2 - L^2}}{2} \quad \text{and for fixed } D, \qquad dr = \frac{-L}{4r}\,dL \tag{4}$$

The frequency of cutting chords of length L from drops of size D is, therefore, calculated as

$$X(L, D) = X(r, D)\left|\frac{dr}{dL}\right| \tag{5}$$

According to Eqs. 3 and 4, Eq. 5 will lead to the following expression:

$$X(L, D) = \frac{\pi}{2} N_T \cdot U \cdot L \cdot P(D) \tag{6}$$

Then the frequency of measuring chord length L from all drops can be calculated by integrating Eq. 6 with respect to the drop diameter, D. We observe that chords of length L cannot be detected from drops whose sizes are smaller than L. So we have

$$X(L) = \frac{\pi U N_T}{2}\int_L^{D_{\max}} L \cdot P(D)dD = \frac{\pi U N_T}{2}\int_0^{D_{\max}} L \cdot P(D)\psi(L, D)dD \tag{7}$$

where $\psi(L, D)$ is defined as

$$\psi(L, D) = \begin{cases} 1, & (L \le D) \\ 0, & (L > D) \end{cases} \tag{8}$$

Consequently, the frequency for the probe to measure chords of any length can be expressed by

$$X_T = \int_0^{L_{\max}} X(L)dL = \int_0^{D_{\max}} X(L)dL \tag{9}$$

where $L_{\max}$ is the maximum chord length and, according to the assumption that drops are spherical and their deformations are negligible, $L_{\max}$ is set equal to $D_{\max}$. Here, X_T represents the overall chord frequency detected by probe. The total number of drops per unit volume, N_T, is a constant provided that the dispersed phase volume fraction and drop size distribution function, $P(D)$, are fixed. Thus, for a given maximum drop size, $D_{\max}$, and average drop velocity, U, the total chord frequency detected by the probe, X_T, will also be a constant. We

define $G(L)$ as the chord length distribution function (CLD) so that the number density of detected chords whose lengths are between L and $(L + dL)$ is $G(L)dL$. If $G(L)$ is estimated from measurements within a time interval Δt, we have

$$G(L)dL = \frac{X(L)dL \cdot \Delta t}{X_T \cdot \Delta t} \tag{10}$$

Hence, the number fraction of measured chord lengths between L_1 and L_2 can be expressed by the following integral:

$$\int_{L_1}^{L_2} G(L)dL = \alpha \int_{L_1}^{L_2} \int_{0}^{D_{\max}} L \cdot P(D)\psi(L, D)dDdL \tag{11}$$

where α is a constant parameter. Equation 11 has the same form as Eq. 1 for $P(L|R)=L/2R^2$ and $P_B(R) \propto R^2$.

Equation 11 can be used to find the likelihood of cutting chord length L ($L_1 \leq L \leq L_2$) for continuous distribution functions. In discrete analysis, if drop sizes are grouped into N categories and chord lengths are grouped into M categories, discretization of Eq. 11 will lead to

$$G(i) = \alpha \sum_{j=1}^{N} f(L_{i-1} : L_i)\, P(j)\psi(L_i, D_j), \quad (i = 1, 2 \cdots M) \tag{12}$$

where $G(i)$ is the number density of chords in the i^{th} chord group; L_{i-1} and L_i are, respectively, the minimal and maximal chord lengths in the i^{th} chord group (L_0 is equal to 0); D_j is the average drop diameter in the j^{th} drop group; $P(j)$ is the fraction of drops in the j^{th} drop group; and the function f is defined by

$$f(L_{i-1} : L_i) = \frac{L_i^2 - L_{i-1}^2}{2} \tag{13}$$

Note that the number of chord-length groups, M, is not required to match the number of drop-diameter groups, N, and that in general $D_i \neq L_i$. Eq. 12 can then be written in the following matrix form:

$$\begin{pmatrix} C(1,1) & \cdots & C(1,N-1) & C(1,N) \\ C(2,1) & \cdots & C(2,N-1) & C(2,N) \\ \vdots & \ddots & \vdots & \vdots \\ C(M-1,1) & \cdots & C(M-1,N-1) & C(M-1,N) \\ C(M,1) & \cdots & C(M,N-1) & C(M,N) \end{pmatrix} \begin{pmatrix} P(1) \\ P(2) \\ \vdots \\ P(N-1) \\ P(N) \end{pmatrix} = \begin{pmatrix} G(1) \\ G(2) \\ \vdots \\ G(M-1) \\ G(M) \end{pmatrix} \tag{14}$$

In compact form, Eq. 14 is written as:

$$[\mathbf{C}][\mathbf{P}] = [\mathbf{G}] \tag{15}$$

where the matrix [**C**] contains the coefficients $C(i,j)$, which are given by

$$C(i, j) = \alpha \cdot f(L_{i-1} : L_i)\psi(L_i, D_j) \tag{16}$$

The forward calculation of the CLD, [**G**], can then be performed directly using Eq. 15, provided that the DSD, [**P**], is known. For the backward calculation of the DSD from the CLD, [**G**], which is given by the experimental data, the number density function, [**P**], can be found from:

$$[\mathbf{P}] = [\mathbf{C}]^{-1}[\mathbf{G}] \tag{17}$$

where the inverse matrix $[\mathbf{C}]^{-1}$ can be obtained directly for $M = N$. However, for cases of $M \neq N$, a singular value decomposition (SVD) algorithm[16] must be used to compute a pseudo-inverse of the non-square matrix [**C**], which minimizes the quadratic form $([\mathbf{G}] - [\mathbf{C}][\mathbf{P}])^{\mathrm{T}}([\mathbf{G}] - [\mathbf{C}][\mathbf{P}])$.

Smoothing equations

As with the methods suggested by previous investigators, Eq. 17 was found sometimes to give negative solutions when applied to experimental CLDs that included noisy errors. To reduce this sensitivity resulting from noisy experimental data, a technique is implemented that has been widely used for solving other inverse problems. Additional smoothing equations are imposed into matrix [**C**] and the inverse of the combined matrix is solved by Tikhonov Regularization.[17-20]

If we know beforehand that the DSD follows a continuous function (such as a log-normal or β distribution, for instance), the drop size number densities between adjacent groups can be assumed to be similar. Hence, we can add the following additional equations into Eq. 15:

$$\lambda_{SF,i}[P(i) - P(i-1)] = 0, \quad i = 2 \cdots N \tag{18}$$

where $\lambda_{SF,i}$ is the *weighting function* for $P(i)$, which controls the extent to which noise in the experimental data is filtered out and the converted DSD curve is rendered smooth. The relationships in Eq. 18 are not enforced as equations, but are enforced in a least square sense by the pseudo-inverse. The appropriate choice of $\lambda_{SF,i}$ has been found to depend on several factors, such as the noise level in the experimental data, the number of groups (M and N), and the actual DSD of the system.[19] The following function is employed for $\lambda_{SF,i}$ in this article:

$$\lambda_{SF,i} = s_f N D_i / D_{\max}, \quad i = 2 \cdots N \tag{19}$$

where s_f is an adjustable dimensionless smoothing factor. The form of Eq. 19 was chosen to ensure that accurate results are obtained for the largest drop sizes. Expressing Eq. 18 in compact form, we have:

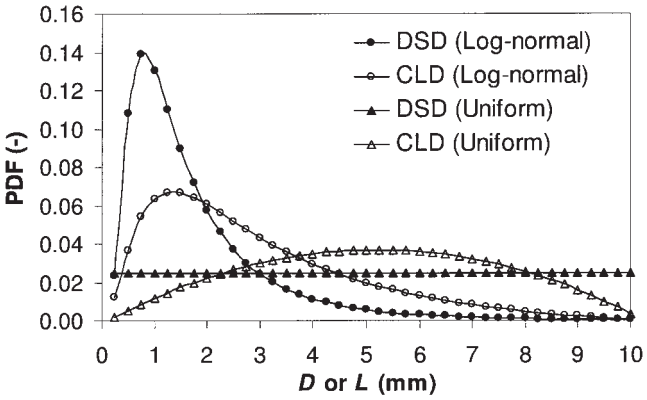

Figure 2. Forward CLD transforms of a log-normal and a uniform DSD.

$$[\mathbf{C}^{\mathrm{S}}][\mathbf{P}] = [\mathbf{0}] \tag{20}$$

where $[\mathbf{C}^{\mathrm{S}}]$ is the coefficient matrix of the smoothing equations with elements given by Eq. 18. Thus, after adding these additional smoothing equations, Eq. 15 is replaced by the following expression:

$$\begin{bmatrix} \mathbf{C} \\ \mathbf{C}^{\mathrm{S}} \end{bmatrix} [\mathbf{P}] = \begin{bmatrix} \mathbf{G} \\ \mathbf{0} \end{bmatrix} \tag{21}$$

The backward conversion from CLD to DSD can, therefore, be obtained in the form:

$$[\mathbf{P}] = \begin{bmatrix} \mathbf{C} \\ \mathbf{C}^{\mathrm{S}} \end{bmatrix}^{-1} \begin{bmatrix} \mathbf{G} \\ \mathbf{0} \end{bmatrix} \tag{22}$$

where the pseudo-inverse is again used.

Results and Discussion

Forward transform from DSD to CLD

Given the system DSD, the CLD can be calculated directly according to Eq. 15. Figure 2 illustrates the forward transform from two continuous DSD functions, the log-normal and uniform distributions, respectively. Here, to maintain the same resolution in the DSD and the CLD, the number of groups of drop diameters and chord lengths are both chosen to be 40. The CLD from the log-normal DSD shows a higher probability at the large sizes (chords) compared to the original DSD, reflecting the sampling bias, while for the system with a uniform DSD a parabolic CLD is obtained.

It is useful to compare the CLD predicted by Eq. 15 with CLD simulated by a Monte-Carlo method. 10^6 drops with a known size distribution were employed within a Monte-Carlo simulation to generate intersected chord lengths. The probability density functions of the chord lengths are shown in Figure 3, where 20 groups of chord lengths are used for drops within the size range of 0-10 mm. Figures 3a and 3b illustrate the results obtained from uniform and (truncated) normal DSDs of the system, respectively. As can be seen, the predictions of Eq. 15 are in good agreement with the Monte-Carlo calculations.

Backward transform from CLD to DSD

While visualization techniques (e.g., endoscopes) can give drop size distribution information directly, other instruments (e.g., impedance or optical probes) will produce only chord length distributions. It is, therefore, necessary to perform the backward calculation to derive the DSD, which is more useful in practice (for example, when the interfacial area of the system is investigated). In this section, two simulations are used to evaluate the method developed above; CLD data are generated either from continuous DSD functions or from Monte-Carlo simulations.

In order to simulate CLD data obtained from experiments, a known DSD was first used to produce an "ideal" CLD, $G(i)$. Then the "ideal" CLD was modified by imposing noise, which leads to:

$$\hat{G}(i) = \zeta[1 + n_l \cdot \kappa]G(i) \tag{23}$$

where n_l is the noise level parameter, κ is a (uniform) random value between 0 and 1, $G(i)$ is the ideal CLD of the i^{th} group, ζ is a normalization constant to maintain $\sum \hat{G}(i) = 1$, and $\hat{G}(i)$ is the noise-added CLD of the i^{th} group.

The CLDs generated from two different continuous distribution functions, the log-normal and uniform distribution (shown in Figure 2), were used first to perform backward calculations. Noisy perturbations with $n_l = 1$ were added into the ideal data, as shown in Figures 4a and 4c. The correspond-

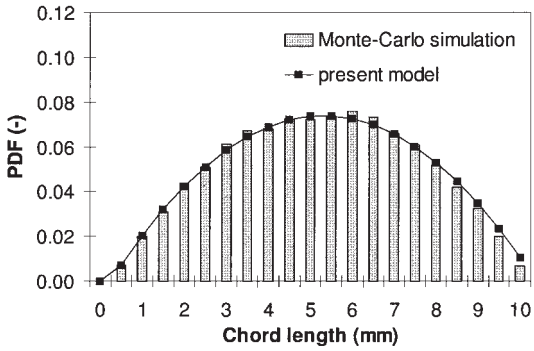

(a)

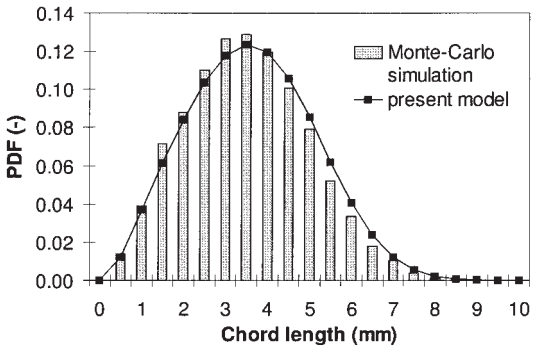

(b)

Figure 3. Comparison of CLD from a Monte-Carlo simulation and prediction by Eq. 15.

(a) Uniform DSD, (b) truncated normal DSD.

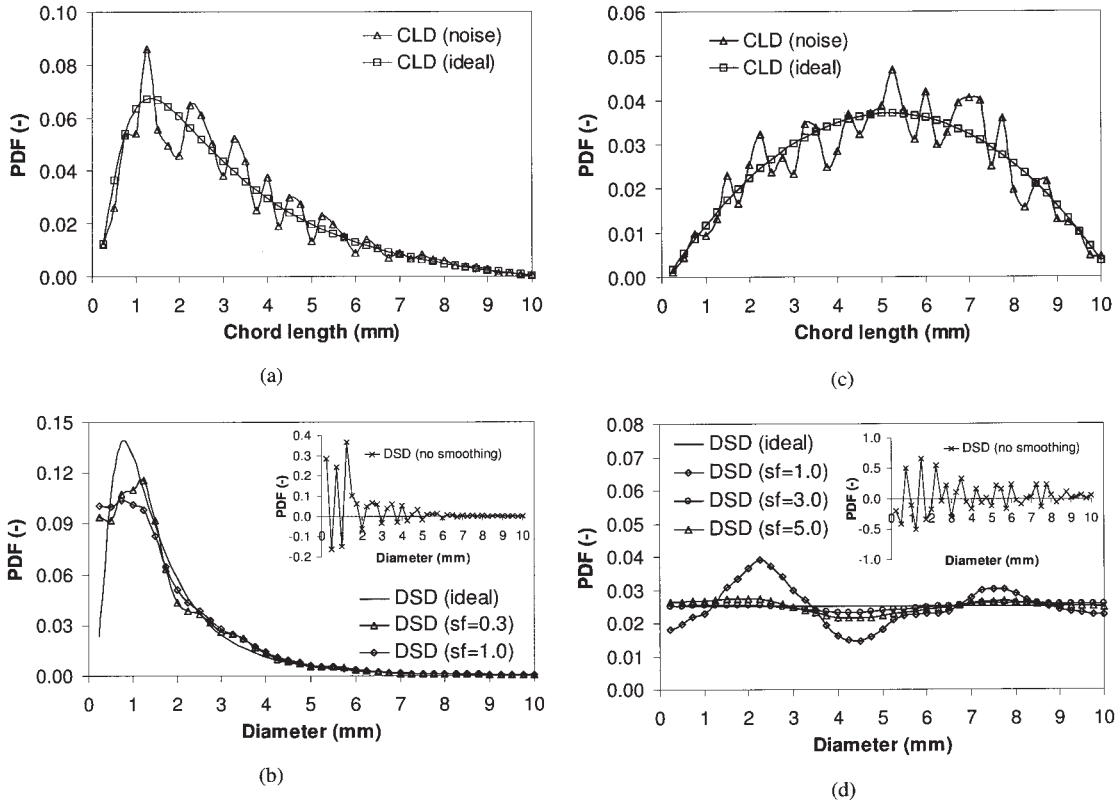

Figure 4. Noise-added CLD and comparison of backward transform for different smoothing factors (s_f).

(a) CLD from log-normal DSD, (b) converted DSD from (a), (c) CLD from uniform DSD, (d) converted DSD from (c).

ing backward conversions, using Eq. 17 without smoothing and Eq. 22 with smoothing, are shown in Figures 4b and 4d and compared with the original DSD. The DSD obtained from Eq. 17 gives many negative values and shows an abnormal curve for both log-normal and uniform distributions. However, after adding the smoothing equations, the DSD results obtained from noisy CLD data showed good agreement with the ideal DSD for the log-normal distribution when smoothing factor $s_f = 0.3$ or 1.0 was applied (see Figure 4b), and for the uniform distribution when $s_f = 3.0$ or 5.0 was applied (see Figure 4d). As pointed out by others,[18,19] the appropriate value of the adjustable parameter s_f was found to depend on the noise level and the distribution type; higher noise and smoother DSD curves require much larger value of s_f. Although the value of s_f is important in obtaining the DSD curve, the converted curve is not sensitive to s_f once the curve is smooth. For example, in Figure 4d, there is a large difference between the results for $s_f = 1.0$ and 3.0, but a much smaller difference between $s_f = 3.0$ and 5.0. In addition, and most importantly, incorporating smoothing into Eq. 22 eliminates the negative DSD values that often occur if the DSD is directly converted from the CLD using Eq. 17. Furthermore, no instability is found in Eq. 22 when the number of size groups is varied.

The Monte-Carlo method was further employed here to evaluate the behavior of the backward transform. Initially, a CLD was generated for a given DSD, either the truncated normal or the uniform distribution (shown in Figure 3), and the backward transform on the CLD was then performed. Figure 5 illustrates the DSD obtained using Eqs. 17 and 22, respectively, without smoothing and with smoothing. As mentioned before, negative values are unavoidable when using direct conversion even if "near ideal" CLD data are used (some differences can be seen between the generated CLD and the ideal CLD in Figure 3). However, when the smoothing equations are added, the converted DSD presents rather good agreement with the original distribution, as can be seen in Figure 5.

Sensitivity studies

As mentioned above, the DSD obtained from the backward transformation of a given CLD using the method proposed in this article depends on several factors, such as the noise level (n_l), the number of DSD groups (N) chosen, and the smoothing factor (s_f). In this section, the sensitivity of the converted DSD to these parameters is further investigated. Figure 6 shows the effect of the number of DSD groups, N, on the generated drop size probability density function. Here, the DSD is obtained by backward transforming noise-loaded CLD data distributed in 40 groups ($n_l = 1$, $M = 40$), originating from a log-normal distribution as shown in Figure 4a, with $s_f = 0.2$. As can be seen in Figure 6, the error in the converted DSD data (open symbols) compared to the ideal distribution (solid symbols) is not strongly dependent on the number of DSD groups used (N) in the range from 40 to 5. This is to be expected because the number of groups N is explicitly factored into the definition of $\lambda_{SF,i}$ in Eq. 19.

The quality of the backward transforms shown in Figure 6 can be further evaluated by the root-mean-square (r.m.s) error, shown in Figure 7, which shows the residual between the ideal and

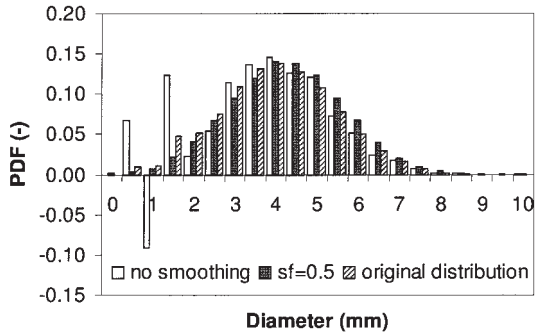

(a)

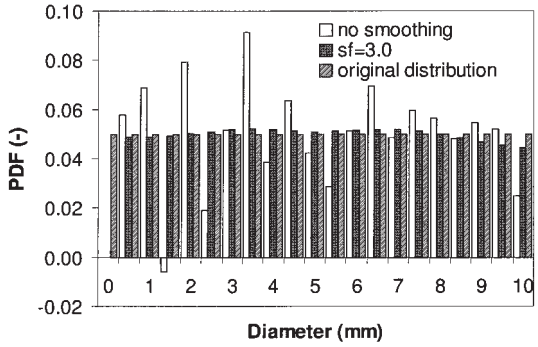

(b)

Figure 5. Backward transform of the CLD generated by the Monte-Carlo method for different smoothing factors (s_f).

(a) Truncated normal DSD, (b) uniform DSD.

converted DSD values, and the relative deviation of a characteristic length scale, in this case, the Sauter mean diameter, $D_{32} = \Sigma D^3/\Sigma D^2$. The r.m.s. and D_{32} deviation are found to increase with decreasing N, indicating a reduction in the quality of the conversion. This discrepancy is also understandable, because the width of the bin becomes larger when N is reduced, so each point represents a wide range of sizes. It can be concluded that in the method developed in this article, a reduction in the DSD resolution does not necessarily improve the estimation of the DSD although

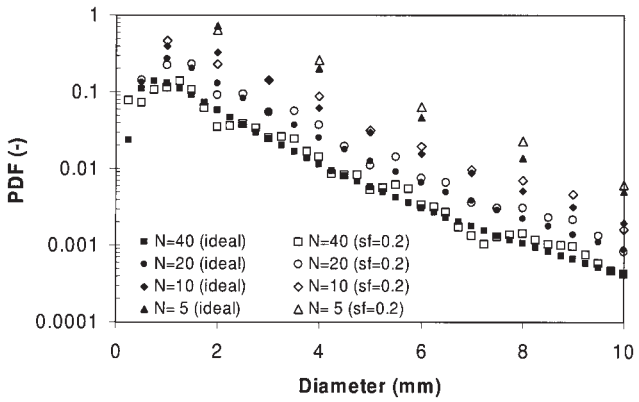

Figure 6. The effect of the number of DSD groups (N) on the converted drop size probability density function.

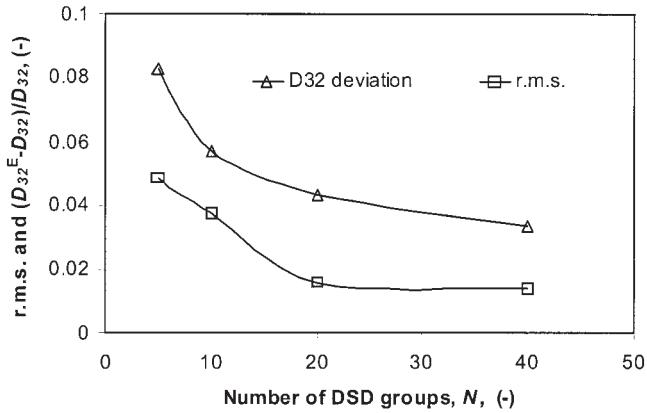

Figure 7. Error between ideal and converted DSD distributions, expressed as r.m.s. and D_{32} deviation for the data shown in Figure 6.

The D_{32} deviation is defined as $(D_{32}^E - D_{32})/D_{32}$, where D_{32} and D_{32}^E are the true and estimated values, respectively.

it may lead to a smoother DSD curve. It is suggested, therefore, that a DSD resolution is used that is at least the same as the CLD resolution, namely $N = M$.

The effect of the smoothing factor value (s_f) on the converted DSD is also investigated. Figure 8 shows the r.m.s. of the residue between the true DSD and the estimated DSD transformed from the CLD with various noise levels and smoothing factors (s_f). The CLD data shown in Figure 4a, obtained from a log-normal drop size distribution, with $N = 40$, are used. As expected, the results in Figure 8 indicate that a larger s_f is required for the CLD data with higher noise level to reach the same r.m.s. level as the less noisy CLD data. Note that even when the ideal CLD data are used, the conversion method developed in this article introduces small errors to the DSD, due to the additional smoothing equations (see $n_l = 0$ in Figure 8). For the noise-loaded CLD data, three distinctive regions can be seen in Figure 8. In the *less-controlled region*, a significant decrease in the r.m.s. values is observed with increasing s_f, but the smoothing equations are less effective in suppressing the noise in the CLD and negative values are often found on the backward transformation. In the *well-balanced region*, the

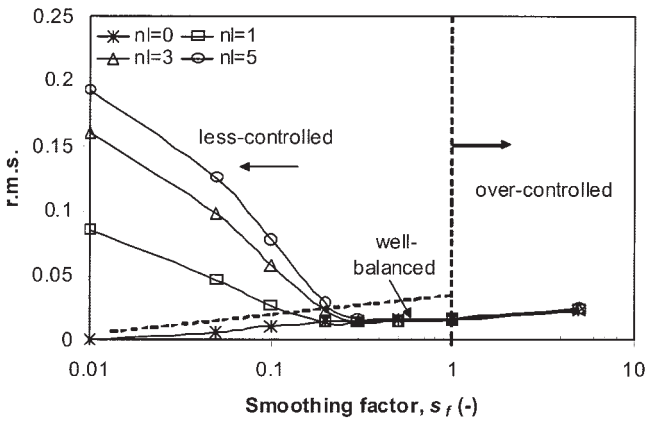

Figure 8. Effect of the noise level (n_l) and smoothing factor (s_f) on the r.m.s. errors for the converted DSD (N = 40, CLD from log-normal DSD as shown in Figure 4a).

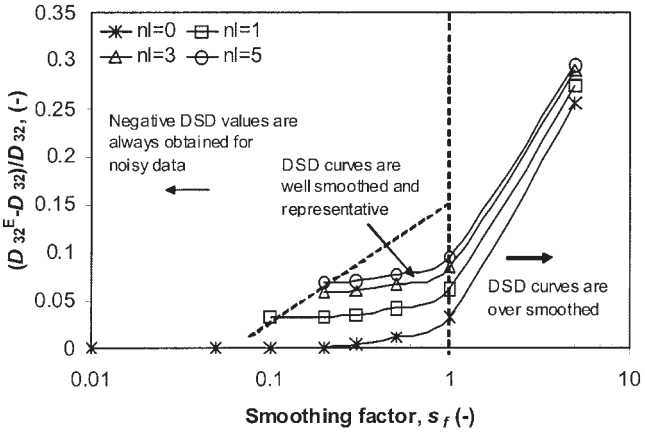

Figure 9. Effect of the noise level (n_l) and smoothing factor (s_f) on the relative deviation of the Sauter mean diameter, estimated from the backward transform (same data as for Figure 8).

r.m.s. values for different noise levels drop down to a low level and reach a minimum at some value of s_f. In this region, the noise in the DSD curve is damped without destroying the form of the curve. Finally, in the *over-controlled region*, the r.m.s. value increases with s_f. At these high values of the smoothing factor, smoothing controls the backward transform so that the noise in the CLD data has negligible effect (the r.m.s. values at different n_l coincide).

For the backward transforms given in Figure 8, the corresponding deviations in D_{32} are shown in Figure 9. Except for the cases in the less controlled region where meaningless negative DSD data are obtained in the other two regions the error in D_{32} increases as a result of imposing the smoothing equations. Two trends can, however, be seen. In the *well-balanced* region, the D_{32} deviation is almost constant for a given level of noise in the CLD, while in the *over-controlled* region there is a significant increase in the D_{32} deviation with the smoothing factor. A smoothing factor in the *well-balanced* region should, therefore, be chosen to get a minimal error in the converted DSD. In practice, however, Figures 8 and 9 are not available unless a direct drop size measuring technique, such as an endoscope, is also used. A good choice of the smoothing factor (s_f) can still be made by plotting the estimated D_{32}^{E} against s_f, which would show a trend similar to Figure 9. The conversion can start with large s_f that decreases gradually until the DSD becomes reasonably smooth and D_{32}^{E} reaches an approximately constant value.

Backward transform from experimental data

Experiments were carried out in vertical dispersed flow of oil and water at 1.5 m/s mixture velocity and 20% oil input volume fraction in a 38 mm I.D. stainless steel tube. A dual impedance probe[4] was employed to measure the chord length distribution of the dispersed oil drops. Simultaneously, a digital camera at 2000 fps was applied to visualize the flow behavior through an acrylic transparent section, and the drop size distribution was measured directly from the video images. Figure 10 shows the cross-sectional averaged CLD obtained from experimental measurements in upward and downward flows, the corresponding DSD estimated by backward transformation with $s_f = 1.0$ (selected using the procedure described above), and the DSD obtained directly from photographic visualization. As can be seen, the predicted DSD obtained from Eq. 22 is closely consistent with the findings from photographic analysis. A large number of small drops (<1.5 mm) were found in the mixture, with large drops observed only occasionally.

Conclusion

In this article, the relationship between the distribution of chord lengths obtained by a needle probe and the distribution of drop sizes in a liquid-liquid dispersion was determined analytically, and a rigorous relationship given by Eq. 12 was developed for spherical drops in uniform motion. The effect of biased sampling towards larger drops, relevant to point sensors, which has often been ignored by other investigators, was included in this relationship. In order to eliminate the negative DSD values that can arise from direct inversion of Eq. 17, smoothing equations were introduced for the DSD functions. Both forward and backward transforms were shown to be in good agreement with ideal data when using continuous (e.g., log-normal, uniform) distributions, and with data obtained from Monte-Carlo simulations. The effect of parameters, such as the noise level, the number of drop size groups used, and the

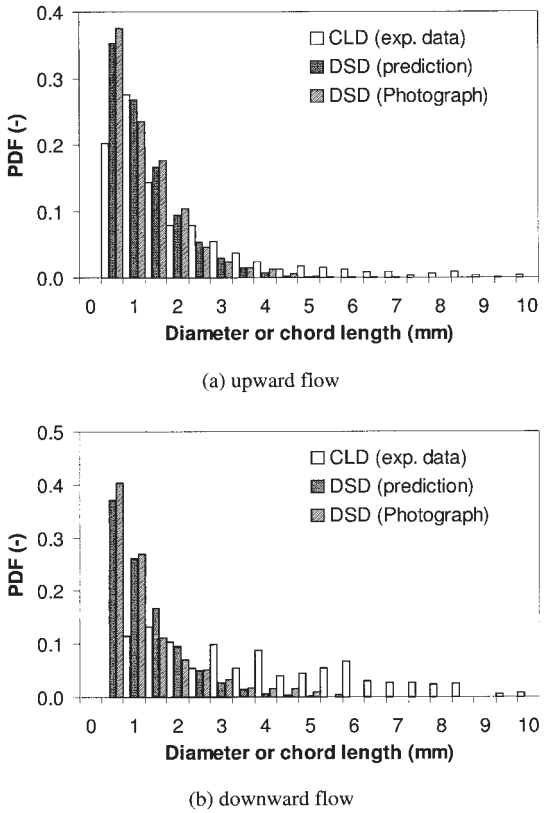

(a) upward flow

(b) downward flow

Figure 10. Experimental CLD data measured using an impedance probe in liquid-liquid dispersions and the corresponding DSD obtained by backward transform with $s_f = 1.0$, in comparison with DSD data from photographic observations.

(a) Upward flow, (b) downward flow.

value of the smoothing factor, on the backward transform were further studied. It was found that the number of drop size groups used can be taken the same as the number of chord length groups to ensure good resolution of the DSD without deterioration of the accuracy; a method for choosing an appropriate smoothing factor, s_f, was also suggested. Finally, drop size distributions converted from experimentally measured chord length distributions showed good agreement with experimental data obtained directly via high-speed photography.

The methodology presented in this article could be generalized to more complicated systems with various dispersed phase shapes and more than one flow direction, for which more complex expressions for $P(L|R)$ and $P_B(R)$ would be needed.

Acknowledgments

The authors gratefully acknowledge financial support from the EPSRC (ref. No. GR/R56044/01). Mr. B. Hu is also grateful to EPSRC and the Overseas Research Students Awards Scheme (Universities UK) for providing financial support. Prof. C. J. Lawrence is grateful to Schlumberger and the Royal Academy of Engineering for their financial support.

Notation

$C(i, j)$ = element of matrix $[C]$ in Eq. 15, dimensionless
D = diameter of drop, m
D_{32} = Sauter mean diameter, m
$f(L_{i-1},L_i)$ = function defined in Eq. 13, m^2
$G(i)$ = discrete chord length distribution of i^{th} category, dimensionless
$G(L)$ = probability of cutting chord of length L, m^{-1}
$\hat{G}$ = noise-added discrete chord length distribution, dimensionless
i = group i of drop size or chord length
j = group j of drop size or chord length
L = chord length, m
M = number of chord-length groups, dimensionless
N = number of drop-size groups, dimensionless
N_T = total number of drops per unit volume, m^{-3}
n_l = noise level, dimensionless
$P(L)$ = probability density of intersecting chord of length L, m^{-1}
$P(L|R)$ = conditional probability of intersecting chord of length L from drop of size R, dimensionless
$P(D)$ = probability density function of drop diameter D, m^{-1}
$P(R)$ = probability density function of drop radius R, m^{-1}
$P_B(R)$ = biased sampling probability function of drop radius R, dimensionless
$P(j)$ = number density of drops in j^{th} group, dimensionless
R = radius of drop, m
s_f = smoothing factor, dimensionless
t = time, s
U = drop velocity, m s^{-1}
$X(r,D)$ = frequency density for drops of size D intersecting probe at center distance r, $s^{-1}m^{-2}$
$X(L,D)$ = frequency density of cutting chord length L from drops of size D, $s^{-1}m^{-2}$
X_T = total frequency of chords intersected by probe, s^{-1}

Greek letters

α = constant in Eq. 11, m^{-2}
ζ = constant in Eq. 23, dimensionless
κ = random number between 0 and 1, dimensionless
λ_{SF} = weighting function defined by Eq. 19, dimensionless
$\psi(L,D)$ = function defined by Eq. 8, dimensionless

Subscripts

i = group i
j = group j
max = maximal value
B = biased sampling
P = sampling distribution
T = total value

Superscripts

E = estimated DSD from backward transform
S = smoothing equation

Literature Cited

1. Kubie J, Gardner GC. Drop sizes and drop dispersion in straight horizontal tubes and in helical coils. *Chemical Engineering Science.* 1977;32:195-202.
2. Angeli P, Hewitt GF. Drop size distributions in horizontal oil-water dispersed flows. *Chemical Engineering Science.* 2000;55:3133-3143.
3. Serizawa A, Kataoka I, Michiyoshi I. Turbulence structure of air-water bubbly flow. Parts I-III. *International Journal of Multiphase Flow.* 1975;2:221-259.
4. Lovick J, Angeli P. Drop size and velocity profiles in liquid-liquid horizontal flows. *Chemical Engineering Science.* 2004;59(15):3105-3115.
5. Wang G, Ching CY. Measurement of multiple gas-bubble velocities in gas-liquid flows using hot-film anemometry. *Experiments in Fluids.* 2001;31:428-439.
6. El-Hamouz AM, Stewart AC. On-line drop size distribution measurement of oil-water dispersion using a Par-Tec M300 laser backscatter instrument. *SPE Journal.* 1996;366672:1-14.
7. Simmons MJH, Langston PA, Burbidge AS. Particle and droplet size analysis from chord distributions. *Powder Technology.* 1999;102:75-83.
8. Clarke NN, Turton R. Chord length distributions related to bubble size distributions in multiphase flows. *International Journal of Multiphase Flow.* 1988;14:413-424.
9. Liu W, Clark NN. Relationships between distributions of chord lengths and distributions of bubble sizes including their statistical parameters. *International Journal of Multiphase Flow.* 1995;21:1073-1089.
10. Liu W, Clark NN, Karamavruc AI. Relationship between bubble size distributions and chord-length distribution in heterogeneously bubbling systems. *Chemical Engineering Science.* 1998;53(6):1267-1276.
11. Langston PA, Burbidge AS, Jones TF, Simmons MJH. Particle and droplet size analysis from chord measurements using Bayes' theorem. *Powder Technology.* 2001;116:33-42.
12. Wynn EJW. Relationship between particle-size and chord-length distributions in focused beam reflectance measurement: stability of direct inversion and weighting. *Powder Technology.* 2003;133:125-133.
13. Hobbel ER, Davies R, Rennie FW, Allen T, Butler LE, Waters ER, Smith JT, Sylvester RW. Modern methods of on-line size analysis for particulate process streams. *Particle & Particle Systems Characterization.* 1991;8:29-34.
14. Santana D, Macías-Machín A. Local bubble-size distribution in fluidized beds. *AIChE Journal.* 2000;46:1340-1347.
15. Kulkarni AA, Joshi JB, Ramkrishna D. Determination of bubble size distributions in bubble columns using LDA. *AIChE Journal.* 2004;50:3068-3084.
16. Press WH, Teukolsky SA, Vetterling WT, Flannery BP. *Numerical Recipes in Fortran 77, The Art of Scientific Computing* (second edition). Cambridge: Cambridge University Press; 1992. pp 51-63.
17. Groetsch CW. *The Theory of Tikhonov Regularization for Fredholm Equations of the First Kind*. Pitman: London; 1984.
18. Nguyen YT, Vu TD, Wong HK, Yeow YL. Solving the inverse problem of capillary viscometry by Tikhonov regularization. *Journal of Non-Newtonian Fluid Mechanics.* 1999;87:103-116.
19. Yeow YL, Nguyen YT, Vu TD, Wong HK. Processing the capillary viscometry data of fluids with yield stress. *Rheol Acta.* 2000;39:392-398.
20. Hu B, Stewart C, Hale CP, Lawrence CJ, Hall ARW, Hewitt GF. Development of an X-ray computed tomography (CT) system with sparse sources: application to three-phase pipe flow visualization. *Experiments in Fluids*. in press.

Manuscript received Dec. 3, 2004, revision received July 8, 2005, and final revision received Sept. 12, 2005.